PAPER Special Issue on Recent Progress in Electromagnetic Compatibility Technology

FDTD Analysis of Dosimetry in Human Head Model for a Helical Antenna Portable Telephone

Jianqing WANG[†] ***and*** **Osamu FUJIWARA**[†]**,** ***Members***

SUMMARY This paper presents a dosimetric analysis in an anatomically realistic human head model for a helical antenna portable telephone by using the finite-difference time-domain (FDTD) method. The head model, developed from magnetic resonance imaging (MRI) data of a Japanese adult head, consists of 530 thousand voxels, of 2 mm dimensions, segmented into 15 tissue types. The helical antenna was modeled as a stack of dipoles and loops with an adequate relative weight, whose validity was confirmed by comparing the calculated near magnetic fields with published measured data. SARs are given both for the spatial peak value in the whole head and the averages in various major organs.

key words: *electromagnetic dosimetry, helical antenna, anatomically realistic head model, FDTD analysis*

1. Introduction

With the rapid and ever more widespread use of portable telephones, public concern regarding the possible health hazards has been growing, which brings an increased requirement on electromagnetic (EM) dosimetry for portable telephones. The basic parameter in the EM dosimetry is defined in terms of the specific absorption rate (SAR), or the absorbed power in unit mass of tissue [1]–[3]. The SAR is generally evaluated using either phantom measurement or computer simulation. The finite-difference time-domain (FDTD) method is currently the most widely accepted means for the SAR computation [4]. This method adapts very well to the human head models which are usually derived from magnetic resonance imaging (MRI) or computed tomography (CT) scans and offers great flexibility in modeling the heterogeneous structures of anatomical tissues and organs. Although various MRI or CT based western head models have been reported [5]–[8], no Japanese one was developed. An anatomically reliable head model is indispensable for a detailed dosimetric analysis.

Moreover, due to the increasing requirement for a smaller dimension and lighter weight of portable telephones, helical antennas are being increasingly used for commercial portable telephones because of their shorter length and comparable radiation performance to the longer monopole antennas. However, few dosimetric analyses have been addressed in the literature. This is because an obvious difficulty is the modeling of helix using usually rectangular FDTD cells. Lazzi and Gandhi have recently proposed a method to model a helical antenna as a stack of dipoles and loops, which does not need modification of the FDTD cell resolution to represent the helix or curved metal wires [8].

In this paper, a dosimetric analysis is performed in an our newly developed MRI-based Japanese head model for an actual portable telephone with helical antenna. The FDTD method is employed in the analysis. The portable telephone is modeled as a plastic covered metal box and the helical antenna is modeled by using the Lazzi and Gandhi proposed method. The validity for the actual portable telephone modeling is first confirmed by comparing the calculated near magnetic fields with measured data published in the literature. Then SARs are given both for the spatial peak value in the whole head and the averages in various major organs. In view of that a portable telephone may not be sufficiently metalized, a dosimetric analysis for a plastic covered shortened metal box with the same helical antenna is also performed.

2. MRI Based Head Model

An MRI based head model was newly developed by our group recently [9]. The raw MRI data were taken from a Japanese adult head (male, 23 years old), which consists of 115 slices with 2 mm apart in the axial plane. Each MRI slice was a 256 × 256 pixel and 9-bit grey scale image. The grey scale data of MRI images were interpreted into tissue types, which is known as a process of segmentation. The segmentation was performed under the guidance of a medical doctor. At first, the grey scale images were rescaled to produce cubical voxel of 2 mm. Then the images were segmented unambiguously as belonging to one of 15 different tissue types by assigning each 2 mm cube voxel to a RGB code which identifies the discrete tissue type of that particular voxel. This process was performed manually with the aid of a commercial software Adobe Photoshop. Care was taken to adjust the fine differences in tissue position between different slices. The segmented tissue types are blood, bone, bone marrow, cartilage, cerebrospinal fluid (CSF), dura, eye tissue, fat, grey matter, lens, mucous membrane, muscle, parotid gland,

Manuscript received July 1, 1999.
Manuscript revised October 2, 1999.

[†]The authors are with the Department of Electrical and Computer Engineering, Nagoya Institute of Technology, Nagoya-shi, 466-8555 Japan.

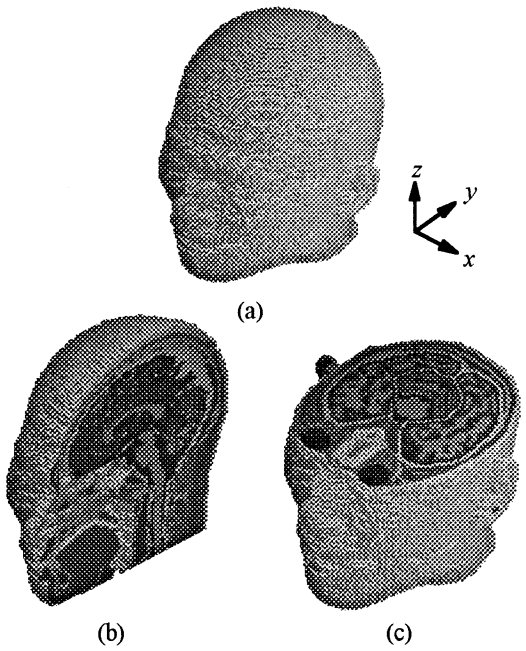

Fig. 1 MRI-based head model. (a) appearance, (b) midsagittal vertical cross-section, (c) horizontal cross-section through the eyes.

Table 1 Dielectric properties of tissue (900 MHz).

Tissue	ρ [kg/m^3]	ε_r	σ [S/m]
blood	1060.0	61.36	1.54
bone	1850.0	16.62	0.24
bone marrow	1030.0	11.27	0.23
cartilage	1100.0	42.65	0.78
cerebrospinal fluid	1010.0	68.64	2.41
dura	1030.0	44.43	0.96
eye tissue	1010.0	55.27	1.17
fat	920.0	11.33	0.11
grey matter	1030.0	52.72	0.94
lens	1100.0	41.21	0.64
mucous membrane	1010.0	46.08	0.84
muscle	1040.0	55.96	0.97
parotid gland	1050.0	60.55	1.21
skin	1010.0	41.41	0.87
white matter	1030.0	38.89	0.59

skin and white matter.

Figure 1 shows the head model, a mid-sagittal vertical cross-section and a horizontal cross-section through the eyes of the head model. The electrical properties for each tissue are cited from [10] and tabulated in Table 1, where ρ is the mass density, and ε_r and σ are the relative permittivity and conductivity, respectively.

3. Helical Antenna Modeling

An actual 900 MHz portable telephone, reported in [11], was modeled by a helical antenna mounted on a plastic covered rectangular metal box. Figure 2 shows the portable telephone model. The metal box was 5.6 cm wide, 2 cm thick, 13.6 cm tall, and the covered plastic case had a thickness of 2 mm and $\varepsilon_r = 2$. The helical antenna had a length $L = 18$ mm, pitch $S = 2$ mm, diameter $D = 4$ mm, and was located at the forward side on the box. Due to the small diameter compared to wavelength, the helical antenna can be considered to be an equivalence of a sequence of dipoles and loops [12]. According to Lazzi and Gandhi's proposal in [8], a rectangular stack, as shown in Fig. 3, to reproduce the fields generated by the sequence of dipole and loops were used to model the helical antenna[†].

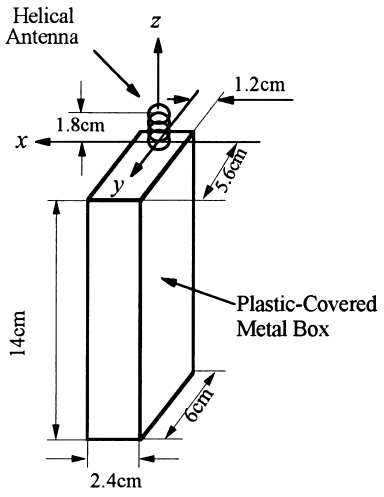

Fig. 2 Model of portable telephone with a helical antenna.

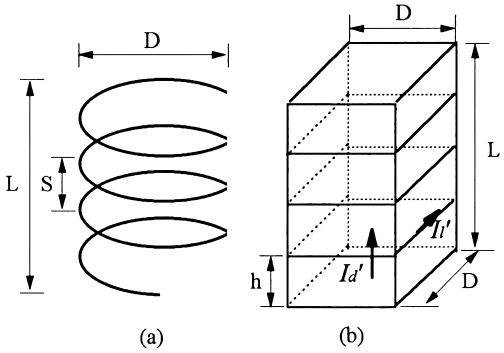

Fig. 3 (a) Helical antenna, (b) stack used to model the helical antenna. The stack is composed of sereval layers. Each layer has a square area with one side equal to the diameter D of the helical antenna, and a height h equal or close to the pitch S of the helical antenna. The height of the stack is equal to the length L of the helical antenna.

Referring to Fig. 3(b), for one layer of the stack, there are an equivalent dipole and an equivalent loop. Denoting the current in the equivalent dipole as I_d', I_d' can be replaced by a displacement current, and the equivalent electric field E_z in lieu of I_d' can be expressed as

[†]The forthcoming description and Eqs. (1)–(5) are based on [8], although the author's explanations are somewhat included.

$$E_z = \frac{I'_d \cdot 1/j\omega C}{h} = \frac{I'_d}{j\omega\varepsilon_0 D^2} \tag{1}$$

where C is the capacitance between the layer, being given by $\varepsilon_0 D^2/h$, and h is the height of each layer.

On the other hand, denoting the current in the equivalent loop as I'_l, from Ampere's law, the equivalent magnetic field related to the current I'_l in the center of the same layer can be expressed as

$$H_z = \oint \frac{I'_l dl' \sin\phi}{4\pi R^2} \simeq \frac{I'_l}{D} \tag{2}$$

where R is the distance from the current element dl' to the center of the layer, ϕ is the angle between the direction of the current and the vector from the element to the center of the layer, and the integration is carried out along the boundary line of the layer.

Thus, for one layer of the stack, we have

$$\frac{E_z}{H_z} = \frac{I'_d}{I'_l}\frac{1}{j\omega\varepsilon_0 D}. \tag{3}$$

Since the stack has a rectangular shape and the height h of each layer may not be identical to the pitch of the helical antenna, it is necessary to relate the currents I'_d and I'_l to I_d and I_l produced by the actual dipole and loop. This was realized by scaling the dipole current by the ratio of the actual and modeled dipole lengths and the loop current by the ratio of the actual and the modeled loop perimeters. Accordingly, we have,

$$I'_d = I_d\frac{S}{h} \qquad \text{and} \qquad I'_l = I_l\frac{\pi D}{4D}. \tag{4}$$

Thus Eq. (3) can be rewritten as

$$\frac{E_z}{H_z} = \frac{4S}{j\omega\varepsilon_0\pi h D} \tag{5}$$

because the current must be continuous on the helix, i.e., $I_d = I_l$. This equation gives the relative weight between the electric and magnetic sources as the excitation.

It is straightforward to model the stack using usual FDTD cells. In this study, 2×2 cells in the xy planes and 9 cells along the z direction were used to model the stack. That means that $S = h$, and $D = 2\ \delta$ in Eq. (5) where δ is the size of cubical FDTD cells. E_z and H_z in the cells modeling the stack were excited sinusoidally according to the relative weight in Eq. (5). Due to each layer of the stack consisted of four cells, the excitation with E_z and H_z was split and assigned as shown in Fig. 4 according to Lazzi and Gandhi's proposal.

To confirm the validity of our modeling for the actual portable telephone, the free space magnetic field H was calculated. Figure 5 shows calculated $|H|^2$ normalized to the maximum $|H|^2$ value at a distance of 5 mm from the portable telephone. Also shown is the measured result reported in [11] by using a magnetic field probe. A good agreement was observed between them, though the calculated values were somewhat larger than the measured ones on the lower part of the box. This result assured that the model is a good representation of the actual portable telephone.

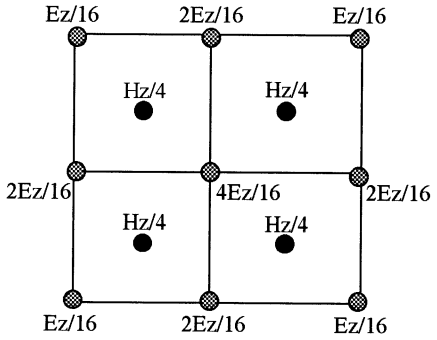

Fig. 4 Excitation method for each layer of the stack modeling the helical antenna.

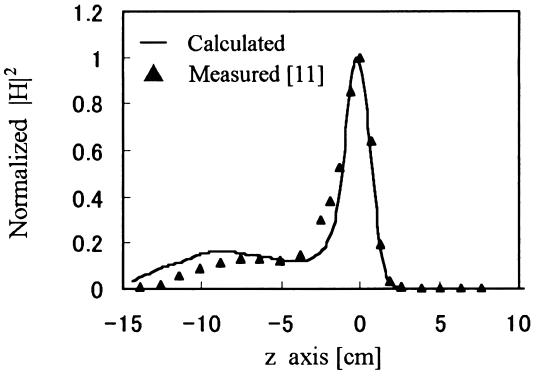

Fig. 5 Calculated and measured squared magnetic fields both normalized to the maximum field values at a distance of 5 mm from the portable telephone.

4. Results and Discussion

For all calculated results given in this section, the antenna output power was set to 0.6 W, which was obtained from the sum of the power absorbed in the head and hand and the power radiated to the far field. The radiated power was calculated by integrating the normal component of the Poynting vector over a surface completely surrounding the configuration of analysis. The hand was simply modeled with 2/3 muscle-equivalent material being 8 cm wide and 2 cm thick and wrapped around three sides of the lower part of the portable telephone. The portable telephone had a vertical alignment at the side of the head by the ear.

4.1 Helical Antenna on a Plastic-Covered Metal Box

As can be seen from the magnetic field distribution shown in Fig. 5, the helical antenna had stronger magnetic fields concentrated in the vicinity of the feed

Table 2 SAR distributions for major organs in the MRI-based head model. The antenna output was 0.6 W.

SAR [W/kg]	helical	quarter-wavelength monopole
One gram peak	2.10	1.78(1.63)*
Ten gram peak	1.21	0.85(0.92)*
Average for whole head	0.049	0.049
One gram peak for brain	1.22	1.08
One gram peak for eye	0.024	0.034
Average for grey matter	0.046	0.049
Average for white matter	0.028	0.030
Average for CSF	0.077	0.078
Average for eye tissue	0.009	0.013
Average for lens	0.002	0.006
Average for parotid gland	0.121	0.089

* SARs for our previous head model [15]

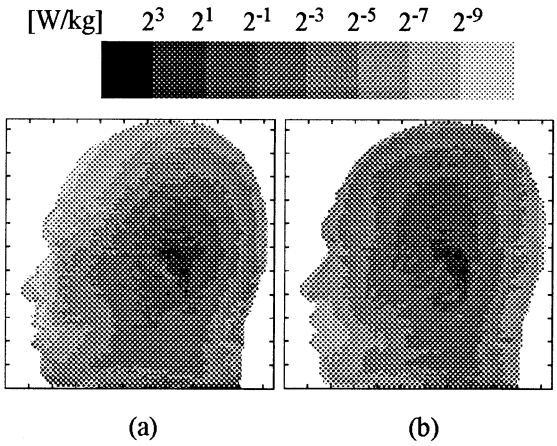

Fig. 6 SAR distributions on the head surface. (a) helical antenna, (b) quarter-wavelength monopole antenna. The antenna output was 0.6 W.

point. Also From Fig. 5, the helical antenna did not effectively choke the RF current on the box which is directly related to the near magnetic field [13]. This means that there may be an increased spatial peak SAR value in the head. Table 2 gives the SAR distributions for major organs in the MRI-based head model with the helical antenna on the plastic covered metal box. For comparison, the SAR distributions in the same MRI-based head model with a quarter-wavelength monopole antenna on a plastic covered metal box are also given. The quarter-wavelength monopole antenna had a radius of 0.5 mm and was located at the same location as that of the helix in Fig. 2. Both the one-gram averaged and the ten-gram averaged spatial peak SARs were obtained over an exact one gram or ten grams of tissue by using a linear interpolation scheme [14]. In addition, the one-gram averaged spatial peak SAR for the brain was obtained over one gram of the grey matter, white matter and CSF, and the one-gram averaged spatial peak SAR for the eye was obtained over one gram of the eye tissue and lens. As expected, an increase in the one-gram averaged and ten-gram averaged spatial peak SARs, say 1.2 times for the one-gram average and 1.4 times for the ten-gram average, was observed with respect to the quarter-wavelength monopole. Moreover, the average SAR in the parotid gland was also increased significantly. But the average SARs in the major organs such as the brain and eyes were lower with respect to the quarter-wavelength monopole. This can be explained by comparing the SAR distributions on the head surface, as shown in Fig. 6, for the two different antennas. Due to the shorter length of helical antenna, the currents concentrated on the antenna and the upper part of the box, that resulted in a concentrated EM absorption in the face area touching the earpiece of telephone. However, with respect to the helical antenna, the peak values were lower but the exposed area was larger for the monopole antenna. The exposed area for the helical antenna was somewhat on the low side relative to the auditory canal, while somewhat on the high side for the monopole antenna, that attributed to the increased average SAR level in the parotid gland and decreased average SAR level in the brain and eyes.

It is difficult to make a direct comparison for the spatial peak SAR with those reported in [8] because different helical sizes, head models and frequencies have been used. Lazzi and Gandhi have reported a one-gram averaged spatial peak SAR of 3.9 W/kg at 835 MHz in [8]. This value is approximately 1.9 times our result at 900 MHz. The reason may be due to a shorter helical length and a pressed-ear head model used in their computation, because pressing the ear by a portable telephone would cause a significant increase in the spatial peak SAR [15].

It is also worthynoting that the one-gram and ten-gram averaged spatial peak SARs are not dissimilar to our previous results obtained from an artificial head model, also developed by our group, with a quarter-wavelength monopole antenna, as given in Table 2.

4.2 Helical Antenna on a Plastic-Covered Shortened Metal Box

In reality a plastic covered portable telephone may not be sufficient metalized to prevent EM interference to the internal circuits from the antenna. A shortened metal box modeling the RF unit inside a plastic case is one choice for representing such a telephone [16]. The shortened metal box may increase the field concentration surrounding the helix and the smaller box. Table 3 gives the SAR distributions for a helical antenna portable telephone with a plastic covered shortened metal box. The modeled portable telephone had the same configuration and size as those in Fig. 2, except that the metal box was shortened to a height of 4.6 cm which was a similar size to a RF unit inside a portable telephone. From Table 3, a significant increase both in the peak SARs and average SARs were found with respect to the normal metal box model. The in-

Table 3 SAR distributions for major organs in the MRI-based head model with a helical antenna on a plastic covered shortened metal box. The antenna output was 0.6 W.

One gram peak	3.25
Ten gram peak	2.23
Average for whole head	0.075
One gram peak for brain	2.30
One gram peak for eye	0.033
Average for grey matter	0.094
Average for white matter	0.057
Average for CSF	0.156
Average for eye tissue	0.012
Average for lens	0.003
Average for parotid gland	0.077

creased factors were 1.5 and 1.8 for the one-gram averaged and ten-gram averaged spatial peak SARs. As an exception, the SAR level in the parotid gland was lower with respect to the normal metal box. This resulted from the highly field concentration and resultant smaller exposed area for the portable telephone with the shortened metal box. For the portable telephone model with a normal metal box, about 30% absorbed power was due to the hand because a RF current flows onto that part of the box. However, for the portable telephone model with the shortened metal box, only 15% absorbed power was due to the hand. The remaining part was absorbed in the head, which attributed to the increased average SAR in the head, brain and eyes. It should be noted that the radiation efficiency for the plastic covered portable telephone model with a shortened metal box was poor, say only 34%.

4.3 Electromagnetic Fields in the Auditory Canal

Due to the field concentration of helical antennas in the vicinity of the auditory canal, it is also possible that a strong field occurs deeper inside the auditory canal. This may cause the electromagnetic interference to hearing aids or artificial inner ears, especially for digital-typed portable telephones [17]. Figure 7 shows the electric and magnetic fields from the entrance to the deepest location of the auditory canal along the x direction for the helical antenna portable telephone with a normal metal box (the model in Fig. 2). As shown in Fig. 7, the electric field E_z dominated over E_x and E_y, which exhibited a standing-wave characteristic. The maximum electric field strength was found to be 146.0 V/m at the entrance of auditory canal, while a comparable strength, say 115.9 V/m, was found deeper inside the auditory canal. The magnetic fields had a dominant component H_y. H_y decreased very slowly with the distance away from the entrance of auditory canal. The maximum magnetic field strength was 0.58 A/m at the entrance of auditory canal. In comparison with a quarter-wavelength monopole exposure reported in [18], the maximum electric field in the auditory canal had a similar level, whereas the maximum magnetic field had a larger value for the helical antenna exposure.

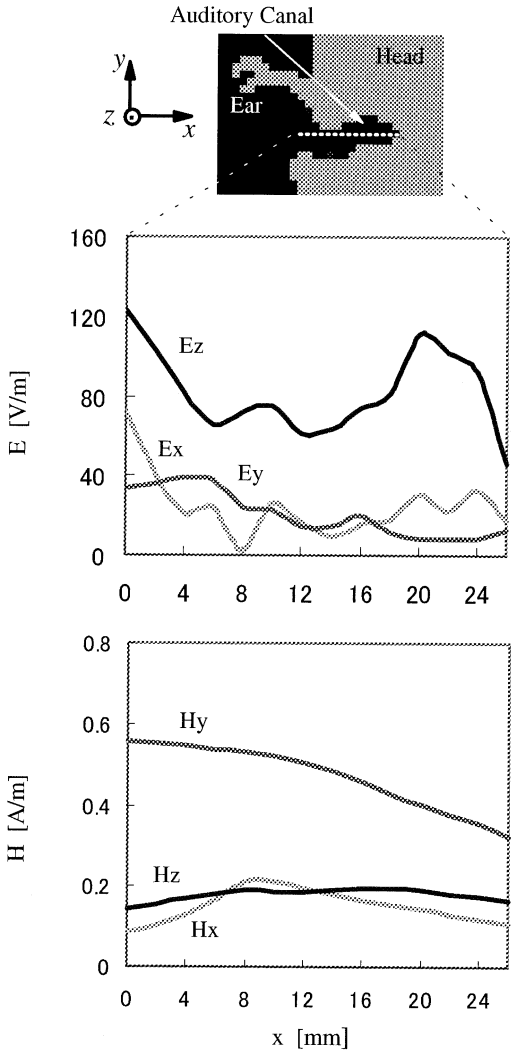

Fig. 7 Electric and magnetic fields from the entrance to the deepest location of the auditory canal. The antenna output was 0.6 W.

5. Conclusions

A dosimetric analysis has been performed in an anatomically realistic human head model for a helical antenna portable telephone by using the FDTD method. The head model has been developed from MRI data of a Japanese adult head, consists of 530 thousand voxels, of 2 mm dimensions, segmented into 15 tissue types. The helical antenna has been modeled as a stack of dipoles and loops with an adequate relative weight. As a result, a higher one-gram averaged or ten-gram averaged spatial peak SAR has been found with respect to a quarter-wavelength monopole antenna, while lower average SARs have been found in the major organs such as the brain and eyes except for the parotid gland. The increased SAR values can be

explained by the field concentration surrounding the shorter helical antenna. A plastic covered shortened metal box has exhibited a stronger field concentration effect, which results in a further increase on the spatial peak SAR in the ear area as well as the SAR values in the brain and eyes. In addition, the electric and magnetic fields inside the auditory canal have also been investigated. The dominant component of electric field exhibits a standing-wave characteristic, while the magnetic field strength decreases with the distance away from the entrance of auditory canal quite slowly.

A further subject is to examine these analytical findings experimentally.

References

[1] American National Standards Institute, "Safety levels with respect to exposure to radio frequency electromagnetic fields, 3 kHz to 300 GHz," ANSI/IEEE C95.1-1992.
[2] International Commission on Non-Ionizing Radiation Protection, "ICNIRP statement—Health issues related to the use of hand-held radiotelephones and base transmitters," Health Physics, vol.70, no.4, pp.587–593, April 1996.
[3] Report of Telecommunications Technology Council for the Ministry of Posts and Telecommunications, Deliberation no.89, "Radio-Radiation Protection Guidelines for Human Exposure to Electromagnetic Fields," Tokyo, 1997.
[4] K.S. Kunz and R.J. Luebbers, "The finite difference time domain method for electromagnetics," Boca Raton, FL, CRC, 1993.
[5] M. Okoniewski and M.A. Stuchly, "A study of the handset antenna and human body interaction," IEEE Trans. Microwave Theory & Tech., vol.44, no.10, pp.1855–1864, Oct. 1996.
[6] V. Hombach, K. Meier, M. Burkhardt, E. Kuhn, and N. Kuster, "The dependence of EM energy absorption upon human head modeling at 900 MHz," IEEE Trans. Microwave Theory & Tech., vol.44, no.10, pp.1865–1873, Oct. 1996.
[7] P.J. Dimbylow, "FDTD calculations of the whole-body averaged SAR in an anatomically realistic voxel model of the human body from 1 MHz to 1 GHz," Phys. Med. Biol., vol.42, pp.479–490, 1997.
[8] G. Lazzi and O.P. Gandhi, "On modeling and personal dosimetry of cellular telephone helical antennas with the FDTD code," IEEE Trans. Antennas & Propag., vol.46, no.4, pp.525–529, April 1998.
[9] T. Ushimoto, J. Wang, and O. Fujiwara, "Dosimetry and its dependence of irradiation direction in MRI based head model for 1.5 GHz microwave far-fields," IEICE Technical Report, EMCJ99-16, June 1999.
[10] C. Gabriel, "Compilation of the dielectric properties of body tissues at RF and microwave frequencies," Brooks Air Force Technical Report AL/OE-TR-1996-0037, 1996.
[11] Q. Balzano, O. Garay, and T.J. Manning, Jr., "Electromagnetic energy exposure of simulated users of portable cellular telephones," IEEE Trans. Veh. Technol., vol.44, no.3, pp.390–403, March 1995.
[12] J.D. Kraus, Antennas, 2nd ed., Ch. 7, McGraw-Hill, New York, 1988.
[13] N. Kuster and Q. Balzano, "Energy absorption mechanism by biological bodies in the near field of dipole antennas above 300 MHz," IEEE Trans. Veh. Technol., vol.41, no.1, pp.17–23, Feb. 1992.
[14] J. Wang and O. Fujiwara, "Uncertainty of the one-gram averaged spatial peak SAR in human head for portable telephones due to average procedures," Trans. IEE of Japan, vol.119-C, no.1, pp.2–8, Jan. 1999.
[15] J. Wang and O. Fujiwara, "FDTD computation of temperature rise in the human head for portable telephones," IEEE Trans. Microwave Theory & Tech., vol.47, no.8, pp.1528–1534, Aug. 1999.
[16] A.D. Tinniswood, C.M. Furse, and O.P. Gandhi, "Computations of SAR distributions for two anatomically based models of the human head using CAD files of commercial telephones and parallelized FDTD code," IEEE Trans. Antennas & Propag., vol.46, no.6, pp.829–833, June 1998.
[17] T. Nojima, Y. Tarusawa, and Y. Suzuki, "Electro-magnetic compatibility of mobile radio communications," NTT DoCoMo Technical Journal, vol.5, no.4, pp.6–14, 1998.
[18] M. Okoniewski and M.A. Stuchly, "Modeling of interaction of electromagnetic fields from a cellular telephone with hearing aids," IEEE Trans. Microwave Theory & Tech., vol.46, no.11, pp.1686–1693, Nov. 1998.

Jianqing Wang received the B.E. degree in electronic engineering from Beijing Institute of Technology, Beijing, China, in 1984, and the M.E. and D.E. degrees in electrical and communication engineering from Tohoku University, Sendai, Japan, in 1988 and 1991, respectively. From 1991 to 1993 and 1995 to 1996, he was with Small Power Communication Systems Research Laboratories Co., Ltd. and Sophia Systems Co., Ltd., respectively, as a Research Engineer. From 1993 to 1995, he was with the Department of Electrical Communication, Faculty of Engineering, Tohoku University, as a Research Associate. He is currently a Research Associate in the Department of Electrical and Computer Engineering, Nagoya Institute of Technology, Nagoya, Japan. His research interests include electromagnetic compatibility, bioelectromagnetics and digital communications.

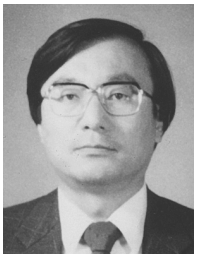

Osamu Fujiwara received the B.E. degree in electronic engineering from Nagoya Institute of Technology, Nagoya, Japan, in 1971, and the M.E. and the D.E. degrees in electrical engineering from Nagoya University, Nagoya, Japan, in 1973 and in 1980, respectively. From 1973 to 1976, he worked in the Central Research Laboratory, Hitachi, Ltd., Kokubunji, Japan, where he was engaged in research and development of system packaging designs for computers. From 1980 to 1984 he was with the Department of Electrical Engineering at Nagoya University. In 1984 he moved to the Department of Electrical and Computer Engineering at Nagoya Institute of Technology, where he is presently a professor. His research interests include measurement and control of electromagnetic interference due to discharge, bioelectromagnetics and other related areas of electromagnetic compatibility. Dr. Fujiwara is a member of the Institute of Electrical Engineers of Japan and of the Institute of Electrical and Electronics Engineers of America.